

PAPER • OPEN ACCESS

Investigations of rotating stall inception in a propeller turbine runner operating in low-load conditions

To cite this article: S Houde *et al* 2019 *IOP Conf. Ser.: Earth Environ. Sci.* **240** 022021

View the [article online](#) for updates and enhancements.

Investigations of rotating stall inception in a propeller turbine runner operating in low-load conditions

S Houde¹, G Dumas¹, Y Maciel¹, C Deschênes¹

¹ Laval University, 1065 Avenue de la Médecine, Québec, QC, G1V 0A6, Canada

E-mail: sebastien.houde@gmc.ulaval.ca

Abstract. This paper presents a study of the inception mechanism of a rotating stall instability identified on a model propeller turbine during speed-no-load (SNL) operation. It seeks to understand the origins of columnar vortices dominating the flow in the runner in SNL. It is based on the use of an experimentally validated flow simulation strategy using the SAS turbulence modelling approach. Two sets of boundary conditions were used to identify the onset of the columnar vortices and confirm that they are linked with a boundary layer separation on the turbine head cover.

1. Introduction

Hydraulic turbines are used more and more to provide spinning-reserve for electrical grids to compensate for the introduction of less reliable energy sources. Spinning reserve requires the turbine to operate at its synchronous rotation speed but without power generation, ready to be linked to the grid in what is termed the speed-no-load (SNL) condition. The turbine's runner flow in speed-no-load is characterized by low discharge and high swirl leading to low-frequency high amplitude pressure fluctuations potentially leading to blade damage and more maintenance downtime [1][2][3][4].

For low-head hydraulic turbines operating at speed-no-load, the large pressure fluctuations in the runner are sometimes attributed to rotating stall [5] [6]. Using embedded pressure transducer measurements, mounted on runner blades of a model propeller turbine, and Scale Adaptive Simulation (SAS) results, Houde *et al.* [7] provided evidence that the rotating stall inception mechanism was linked with columnar vortices, attached to the head cover in the vane less space, rotating in precession with the runner. However, the origins of those columnar vortices could not be clearly identified.

Such structures were observed experimentally by Pulpitel *et al.* [8] in a low-head turbine model of similar configuration at the speed-no-load conditions and its vicinity. They postulated that those structures originated from the reorganization of vorticity generated by a shear layer which itself was the consequence of a large backflow at the draft tube center extending upstream past the runner hub. Houde *et al.* [7] proved that the origins of those vortical structures was independent of the runner blades themselves, i.e. they can exist without the runner blades being present, confirming findings by Bettochi *et al.* [9].



This paper is a follow-up study on the origins of those vortical structures. Relying on the flow simulation strategy validated in speed-no-load conditions, this paper explores the parametric operating space of a propeller turbine in low-load conditions to determine the onset and growth of the instability associated to the formation of coherent columnar vortices, and by the same occasion confirm or refute Pulpitel *et al.* [8] hypothesis.

2. Flow dynamics in speed-no-load conditions

Constant speed reaction hydraulic turbines operate in no-load conditions during a normal start-up sequence. Speed-no-load (SNL) is the final part of this sequence in which the turbine has reached the generator synchronous rotation speed (n_s) while delivering no net torque (T_{gen}) under a given net Head (H) and discharge (Q). On the efficiency $\eta = T_{gen}n/\rho EQ$ hill chart, where $E=gH$, of a particular turbine with a reference diameter D , using the dimensionless blade speed ($n_{ED}=nD/E^{0.5}$) and discharge ($Q_{ED}=Q/DE^{0.5}$) parameters, the no-load line (also referred to as “Runaway line”) corresponds to $\eta=0$ with $T_{gen}=0$. Typically, SNL conditions are associated with low discharge and small guide-vane opening angles (α) where the ratio between the angular momentum and discharge at the runner exit is high with respect to normal operating conditions.

Such swirl dominated flows are often unstable, leading to flows in the main parts of the turbine described as dominated by “stochastic” fluctuations [10] [11]. However, some studies in no-load conditions have identified dominant coherent flow features. Two frequently recurring observations on flow dynamics in no-load regimes are large flow separations extending from the runner entrance to the draft tube and the presence of inter-blade channel vortices [11] [12][13][14]. For some turbines, speed-no-load conditions have also been linked to the onset of what is termed “rotating stall” [12] [15] [16] [17]. In hydraulic turbines, this phenomenon is only documented for operation near the no-load conditions and often refers to flow separations associated with unfavourable angles of attack on the rotor blades leading to the formation of vortices and blockage of inter-blade channels [12] [15] [16].

Pulpitel *et al.* [8] observed on a model Kaplan turbine, operated in no-load conditions, vane-less space vortices in precession with the runner that were generally stable and took different configurations depending on the operating parameters of the no-load conditions. They were also associated with backflows extending into the draft tube. Their visualizations indicate stable configurations of either 3 or 4 vertical vortices attached to a fixed circumferential vortex in the vane-less space. Their hypothesis on the origin of this flow configuration hinged on the presence of the shear layer arising from the backflow cells extending to the vane-less space in high swirl conditions.

2.1 AxialT flow dynamics in speed-no-load

SNL was studied both experimentally and numerically in the AxialT project. The AxialT turbine model has a semi-spiral casing, a distributor with 24 stay-vanes and guide-vanes, a 6 blades propeller runner with a 0.8 specific speed, and a single pier bended draft tube (Figure 1). The scale model was set up on the LAMH turbine test rig. This test rig consists of a classical closed-loop hydraulic facility with flow rate up to 1 m³/s, head up to 50 m, and a maximal net power output of 170 kW. More details on the turbine can be found in Houde *et al.* [7].

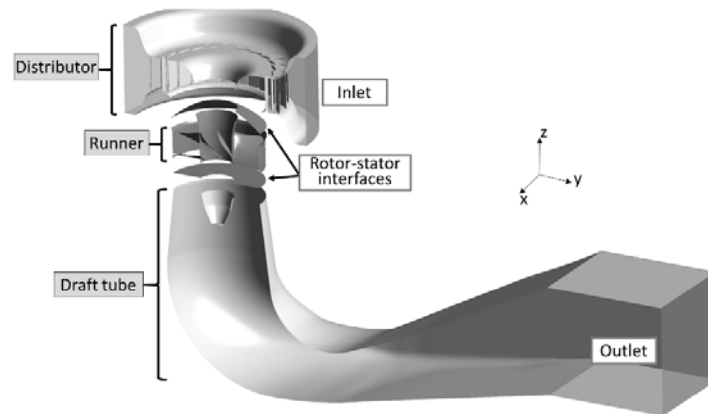


Figure 1. AxialT computational domains. Boundary conditions locations used for simulations are indicated.

The guide vanes opening for the SNL conditions represents 20% of the full load opening. The speed-no-load conditions were studied as part of a larger investigation into transient regimes [18]. The main investigating tools were 31 piezo resistive pressure transducers mounted on two runner blades. Pressure and operating conditions (Q , H , n) were recorded in two different transient scenarios linked to the SNL conditions: Run 1 going from SNL to full-load and Run 2 going from full-load to SNL (Figure 2).

A spectral analysis of the pressure signals during both runs was made using wavelet routines. Figure 3 shows results for a sensor located near the middle of the leading edge on the pressure side of one blade. The largest fluctuations occur in the speed-no-load regime. That energy is spread mainly in the sub-synchronous range ($\log[f/n] < 0$). One frequency stands out among the others, $f/n=0.88$, which carries a higher energy level over the entire SNL range. Interestingly, that frequency also dominates in low-load regime just before and after the no-load conditions.

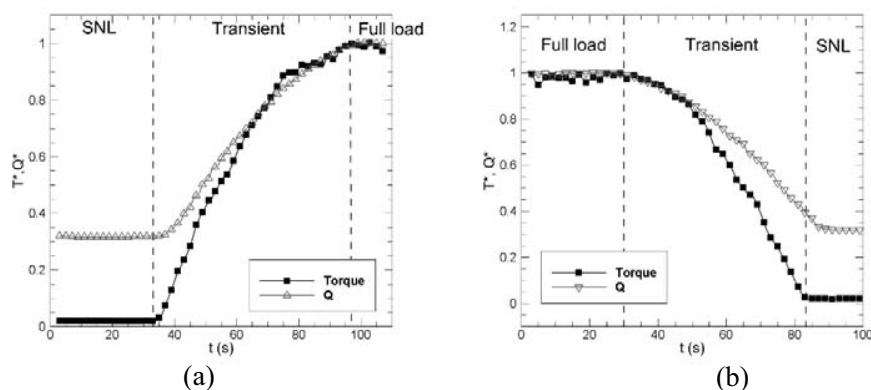


Figure 2. Measured normalized discharge (Q^*) and torque (T^*) of AxialT:
a) **Run 1** from SNL to full load; b) **Run 2** from Full load to SNL.

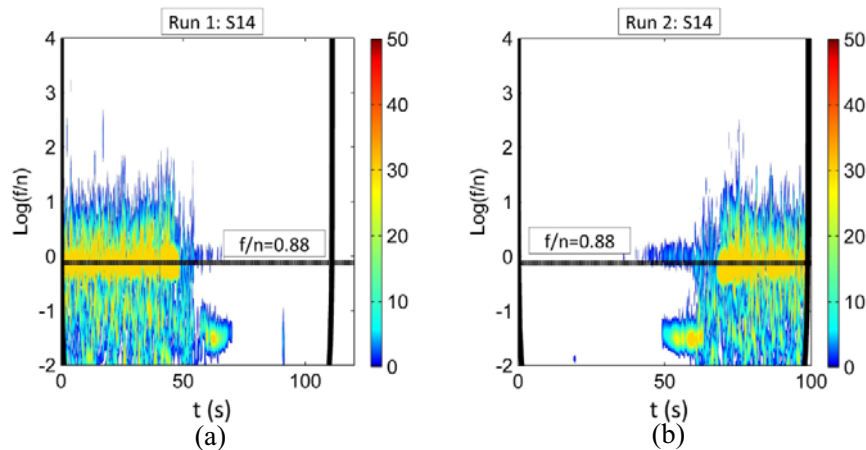


Figure 3. Wavelet analysis for sensor S14: a) Run 1; b) Run 2.

Scale Adaptive Simulations (SAS) were validated against those pressure measurements in Houde *et al.* [7]. They revealed that the $f/n=0.88$ component is associated with three vortices rotating in precession with the runner. Those vortices are attached to the head cover in the vane-less space and extend in the inter blade channel up to the runner exit. Each vortex is associated with a backflow region that also extends from the head-cover to the runner channel and induces what is defined as a rotating stall. At the runner exit, the backflow regions are present in all 6 channels and a large re-circulating region exist under the runner hub deep into the draft tube.

Simulations in the same conditions but without the runner blades still yielded the vortical structures and their associated backflow (Figure 4a). This confirms that the rotating stall inception mechanism is independent of the runner blades themselves and that the runner merely interacts with vortical structures generated upstream of itself. The simulations showed a boundary layer separation on the head cover (Figure 4b) and the presence of a large backflow region around the runner hub both yielding vorticity layers potentially associated with the columnar vortices.

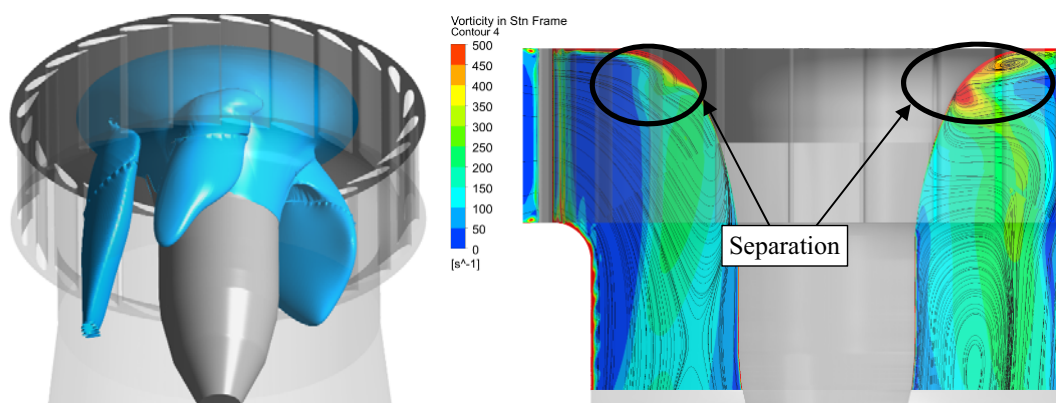


Figure 4. a) Iso surface of pressure illustrating the columnar vortices. b) Contours of vorticity and pseudo-streamlines on a YZ plane illustrating flow separation on the head cover of the studied turbine.

3. Methodology

In order to identify the origin of the rotating stall in the AxialT turbine a new set of simulations were performed at different flow conditions for two n_{EQ} - Q_{ED} characteristic curves associated with a constant guide vanes opening (α) corresponding to the SNL conditions measured on the model. Those two curves were obtained by variations of the rotation speed and discharge. The objectives of the tests were to:

1. Identify the inception point of the instability on the characteristic curves.
2. Assess the influence of the runner rotation speed, and consequently of the runner, on the inception mechanism.

The second objective entails that, by varying independently Q and n on the same n_{EQ} - Q_{ED} characteristic curve, one should get different solutions. The simulations set resulting from Q variations at constant n is tagged Q_v while the set performed at constant Q with varying n is tagged n_v .

3.1. Computational domain and spatial discretization

The computing domains are illustrated in Figure 1. The semi-spiral casing was omitted from the simulations but the stay-vane channels include a converging section representing the mid-section of the semi-spiral casing. The guide-vane angle corresponds to a low-load SNL condition on the AxialT turbine. The interface between the runner and the guide vanes is located on a cross-stream surface about mid-way between the guide-vane trailing edges and the runner blade leading edges.

The computational grids of all components are based on structured hexahedral elements. The meshes of all components were checked to deliver a grid influence of less than 5% on the individual component head losses and less than 1% on the stay vanes, guides vanes and runner blades torque. Results of the runner grid convergence shows that the selected mesh delivers results within the “mesh independent” range for torque prediction. The total number of elements was 15.8 M. More details are provided in Houde et al. [7]

3.2. Boundary conditions and solver parameters

The boundary conditions are adapted from those used in the SNL simulations [6]. They are presented in Table 1 for both simulations sets. The inlet values of turbulent kinetic energy and turbulent viscosity (ν_t) came from spiral casing simulations and were kept constant for all simulations. Distributor/runner and runner/draft tube interfaces are time-dependent rotor-stator interfaces.

Table 1. Boundary conditions for the n_v and Q_v simulation sets. The values are normalized with the discharge and rotation speed at speed-no-load (Q_{SNL} , n_{SNL}).

n/n_{SNL}	Q/Q_{SNL}	n/n_{SNL}	Q/Q_{SNL}
n_v		Q_v	
0.85	1.00	1.00	1.11
0.66	1.00	1.00	1.26
0.55	1.00	1.00	1.47
0.39	1.00	1.00	1.68
0.28	1.00	1.00	2.21

The solver used is ANSYS CFX v18.2. The time integration scheme is based on a second-order implicit Euler formulation. The time step (Δt) used in the SNL simulations corresponds to 1° of runner rotation. The so-called “High Resolution” scheme was chosen for the advection part of the momentum equations. This scheme adjusts a blend factor (β) between a purely first order upwind scheme ($\beta=0$) and a second order upwind scheme ($\beta=1$) depending on mesh quality and local flow dynamics. For the SNL simulations, the scheme delivered an averaged value of $\beta=0.9$ over the entire simulation domain.

The simulations were performed sequentially on both characteristics curves, starting from the SNL conditions and using the solution from the previous operating point as an initial condition. This procedure entails that the flow history is carried over from point to point on the characteristic curves and each simulation starts with the fully develop flow instability at the runner entrance from the previous run. Such initial conditions thus mimic what could be done on a test stand to cover the parametric space from SNL.

4. Results

Figure 5 presents the normalized $n_{ED}^*-Q_{ED}^*$ characteristic curves obtained from the simulations. The normalization is performed with respect to the values at SNL ($n_{ED}^*=1$). Both sets of simulations delivered quite similar curves considering the limited physical time on which they are based. Results on the n_v and Q_v curves are thus expected to have similar kinematic flow behaviour albeit at different head. The torque increase in both scenarios (Figure 5b) confirms that the turbine is moving away from the SNL conditions as n_{ED}^* decreases.

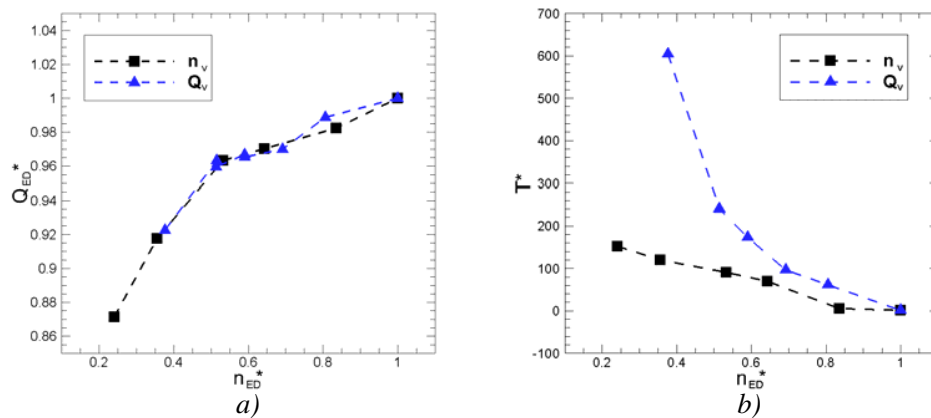


Figure 5. Numerical characteristic curves for the Q_v and n_v sets: a) $n_{ED}^*-Q_{ED}^*$, b) $n_{ED}^*-T^*$.

A comparison of the flow topology for $n_{ED}^*=1$ and the minimum n_{ED}^* of both the n_v and Q_v curves is presented in Figures 6, 7 and 8. The backflow and vorticity in the inter-blade channel and the backflow in the draft tube conical diffuser serve to illustrate the evolution of the columnar vortex instability with respect to the operating conditions. Essentially, intense vorticity regions are still present in the vane-less space and are associated with backflow for all simulations. In the n_v case, this vorticity still reorganize itself into somewhat coherent structures equating columnar vortices. For the Q_v case, at the minimum n_{ED}^* , the flow does not reorganise itself into easily detectable columnar vortices. On the pressure signal this translates into what can be described as low frequency stochastic fluctuations. The backflow in the vane-less space is still present for all cases and extends to the head cover where it is associated with a boundary layer separation.

Interestingly, in both scenarios, the large backflow regions present around the hub in the draft tube at SNL (Figure 8) is absent.

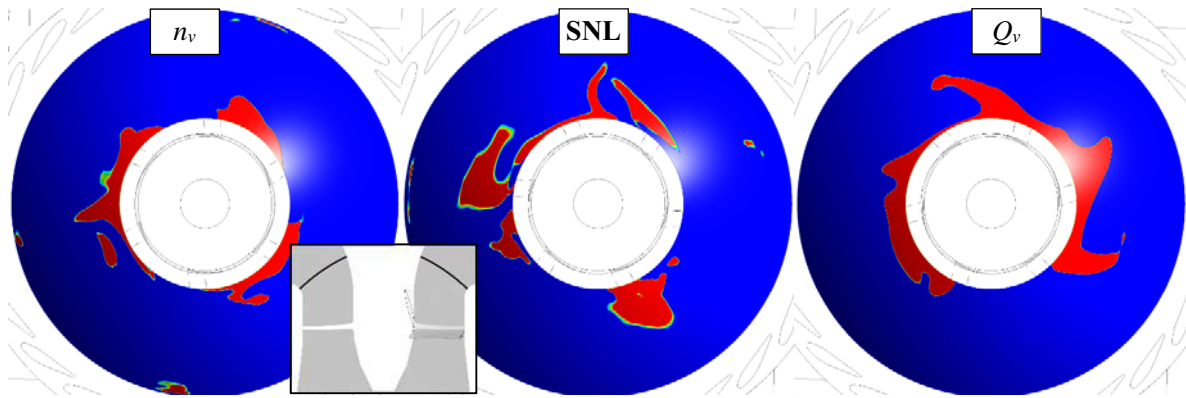


Figure 6. Backflow in red in the vane-less space for the speed-no-load condition (SNL) and the minimum n_{ED}^* values of the n_v and Q_v simulation sets.

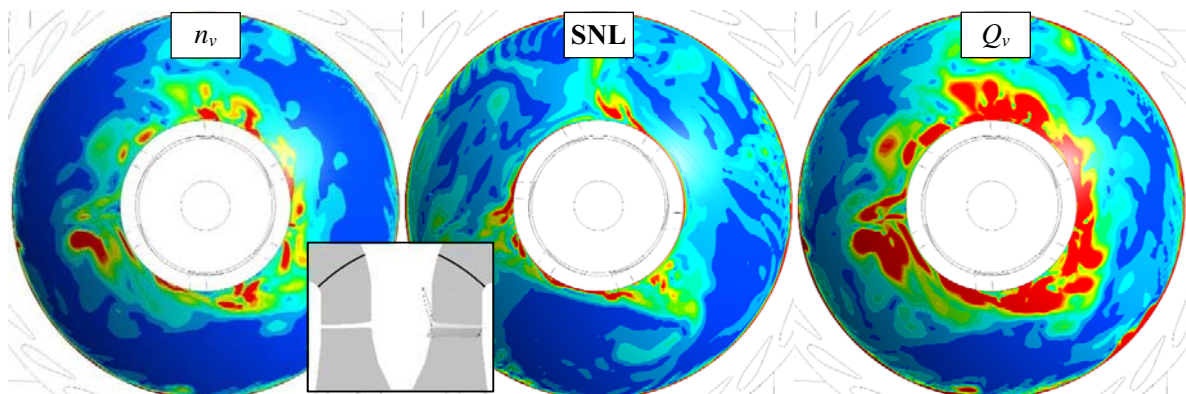


Figure 7. Vorticity module in the vane-less space for the speed-no-load condition (SNL) and the minimum n_{ED}^* values of the n_v and Q_v simulation sets. Regions in red have the highest intensity.

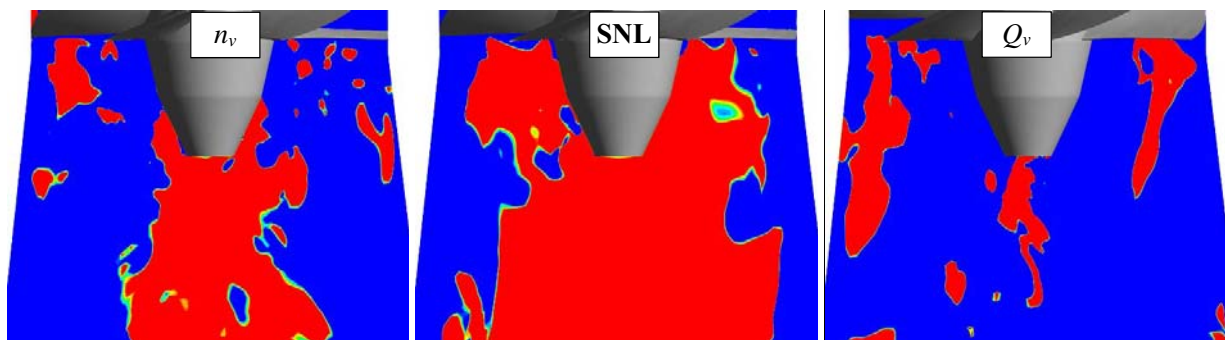


Figure 8. Backflow (in red) in the draft tube conical diffuser on a ZX plane for the speed-no-load condition (SNL) and the minimum n_{ED}^* values of the n_v and Q_v simulation sets.

In order to identify an inception point, Table 2 presents an overview of flow characteristics related to the number of columnar vortices present in the inter-blade channels and the presence of the central draft tube backflow. The number of vortices in the vane-less space is quite different with respect to the selected n and Q . In both scenarios, as the operating conditions moves away from *SNL* conditions, the number of columnar vortices tend to increase leading to configurations of 4 to 6 vortices. Once the number of columnar vortices reaches 6 (figure 9), the relative speed of those structures with respect to the runner is 0 and no dominant peaks can be detected from spectral analysis of the blades pressure signals, hence rotating stall is absent although a large backflow is still present, extending from the head cover to the runner exit.

Table 2. Overview of the flow characteristics for the n_v and Q_v simulation sets.

n_{ED}^*	Columnar vortex	Draft tube backflow	n_{ED}^*	Columnar vortex	Draft tube backflow
n_v			Q_v		
0.24	3 to 5	No	0.38	6	No
0.35	3 to 5	No	0.52	5 to 6	No
0.53	3 to 4	Yes	0.59	3 to 4	Yes
0.64	3 to 4	Yes	0.69	3 to 4	Yes
0.84	3	Yes	0.81	3	Yes
1.0 (SNL)	3	Yes	1 (SNL)	3	Yes

Interestingly, the number of coherent vortices with respect to n_{ED}^* differs in both Q_v and n_v sets suggesting that the flow dynamics is not simply related to the n_{ED} number or to the runner rotation speed. A swirl number was calculated at the distributor exit for the different simulations but did not yield any obvious correlation with the evolution of the flow dynamics.

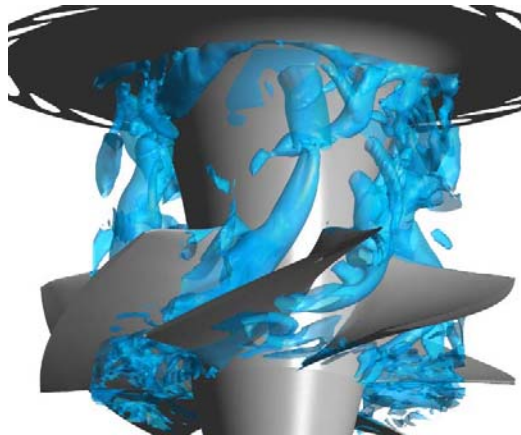


Figure 9. Columnar vortices in the runner for the Q_v case at $n_{ED}^*=0.38$ identify through a Q criterion.

More importantly, the backflow in the conical diffuser decreases in size until it disappears in both scenarios as shown in Figure 8. However, the columnar vortices are still present, albeit in less stable configurations. This does indeed confirm that the origin of the instability does not lie with a shear layer generated by this backflow. However, in all simulations, boundary layer separations occur on the head cover

in the vane-less space pointing out the most likely origin of the columnar vortices. Hence, it appears that the large draft tube backflow observed in the SNL conditions is not associated with the presence of the columnar vortices an observation which, somehow, invalidates Pulpitel *et al.* [8] hypothesis on the origin of the columnar vortices.

The inception point of the columnar vortices is not so easily defined using the simulation sets since in all studied cases there is still flow separation on the head cover and intense vorticity regions in the vane-less space. However, considering that for the Q_v set at $n^*_{ED}=0.38$ the number of columnar vortex precludes the detection of rotating stall, one might consider that a loosely defined inception point should lie between $n^*_{ED} = 0.38$ and 0.52 where the flow transitions to a stable configuration of 6 vortices. Stability analysis of a simplified model flow would be useful to uncover the exact physical mechanism at play.

Conclusion

The study presented in this paper aimed at identifying the inception mechanism of a rotating stall instability present in a propeller turbine in speed-no-load conditions. It was already demonstrated by Houde *et al.* [7] that this rotating stall was associated with columnar vortices in precession with the runner and originating in the vane-less space between the distributor and runner. Those vortices are associated with backflow regions inducing the observed rotating stall. Using two sets of simulations it was possible to isolate the inception mechanism of the rotating stall and link it to a boundary layer separation on the head cover in the vane-less space. The simulations results disprove the hypothesis linking the unstable vorticity distribution, associated with the columnar vortices, to a large backflow present in the draft tube at speed-no-load. However, if the origin of the vorticity leading to the columnar vortices is indeed a boundary layer separation, the evolution of that vorticity is dependent on the operating conditions and can also lead to apparently stochastic fluctuations with no dominant flow structures. Fundamental studies on simplified test case are needed to study the exact mechanisms leading to the boundary layer separation and to the re-organization of the flow into the structures observed in the speed-no-load conditions. Ultimately, such results could be used to minimize the impact of the speed-no-load regime on the turbine service life.

Acknowledgments

The authors would like to thank the participants on the Consortium on Hydraulic Machines for their support and contribution to this research project: Andritz Hydro Canada Inc., GE Renewable Energy, Hydro-Québec, Laval University, NRCAN, Voith Hydro Inc. Our gratitude goes as well to the Canadian Natural Sciences and Engineering Research Council who participated in the funding for this research and to Compute Canada who provided the necessary computing allocations resources.

Nomenclature

n = turbine rotation speed [rev/s]

T = torque [Nm]

H = Net head available for extraction [m]

E = specific energy = gH [J/kg]

Q = Discharge [m^3/s]

D = Turbine reference diameter [m]

g = gravity [m/s^2]

ρ = fluid density [kg/m^3]

Q_{ED} = discharge parameter [-]

n_{ED} = blade speed parameter [-]

α = guide vanes opening angle [$^\circ$]

t = time [s]

T^*, Q^* = normalized torque and discharge [-]

P = pressure [kPa]

P_n = normalized pressure [-]

f = frequency [Hz]

$E_k(-)$ = Spectral energy [-]

k , TKE = turbulence kinetic energy [m^2/s^2]

ν_t = turbulence viscosity [m^2/s]

Δt = simulation time step [s]

β = CFX advection scheme blend factor [-]

References

- [1] Seidel U., Mende C., Hübner B., Weber W., Otto A., 2014, “Dynamic loads in Francis runners and their impact on fatigue life”, proc. of 27th IAHR Symposium on Hydraulics Machinery and Systems, Montreal, Canada.
- [2] Huang, X., Chamberland-Lauzon J., Oram C., Klopfer A., Ruchonnet N., 2014, “Fatigue Analyses of the Prototype Francis Runners Based on Site Measurements and Simulation.”, IOP Conference Series: Earth and Environmental Science, IOP Publishing, <http://iopscience.iop.org/1755-1315/22/1/012014>.
- [3] Hübner B., Weber W., Seidel U., 2016, “The role of fluid-structure interaction for safety and lifetime prediction in hydraulic machinery”, proc. of 28th IAHR Symposium on Hydraulics Machinery and Systems, Grenoble.
- [4] Nennemann B., Morissette J.F., Chamberland-Lauzon J., Monette C., Braun O., Melot M., Coutu A., Nicolle J., Giroux A.-M., 2014, “Challenges in Dynamic Pressure and Stress Predictions at No-Load Operation in Hydraulic Turbines”, IOP Conference Series: Earth and Environmental Science, **22**, 3.
- [5] Botero, F., V. Hasmatuchi, S. Roth, and M. Farhat., 2014, “Non-Intrusive Detection of Rotating Stall in Pump-Turbines”, Mechanical Systems and Signal Processing, **48**, 162–73.
- [6] Nicolle J., Giroux A.-M., Morissette J.-F., 2014, “CFD Configurations for Hydraulic Turbine Startup”, IOP Conference Series: Earth and Environmental Science **22**, **3**.
- [7] Houde S., Dumas G., Deschênes C., 2018, “Experimental and numerical investigations on the origins of rotating stalls in a propeller turbine runner operating in no-load conditions”, Journal of Fluid Engineering, **140**, 11, doi: 10.1115/1.4039713.
- [8] Pulpitel L., Skotak A., Koutnik S., 1996, “Vortices rotating in the vaneless space of a Kaplan turbine operating under off-cam high swirl flow conditions”, proc. of 18th IAHR Symposium on Hydraulic Machinery and Systems, Valencia, Spain.
- [9] Bettocchi R., Cantore G., Magri L., Ubaldi M., 1982, “Analyse experimental de l’écoulement dans la zone axiale des canaux adducteurs des turbines-hélices”, La Houille Blanche, **7/8**.
- [10] Morissette J.-F., Chamberland-Lauzon J., Nennemann B., Monette C., Giroux A.-M., Coutu A., Nicolle J., 2016, “Stress predictions in a Francis turbine at no-load operating regime”, proc. of 28th IAHR Symposium on Hydraulics Machinery and Systems, Grenoble.
- [11] Mende C., Weber W., Seidel U., 2016, “Progress in load prediction for speed-no-load operation in Francis turbines”, proc. of 28th IAHR Symposium on Hydraulics Machinery and Systems, Grenoble.
- [12] Nicolle J., Giroux A.-M., Morissette J.-F., 2014, “CFD Configurations for Hydraulic Turbine Startup”, IOP Conference Series: Earth and Environmental Science **22**, **3**.
- [13] Li Z., Huili B., Zhengwei W., Ze Y., 2016, “Three-Dimensional Simulation of Unsteady Flows in a Pump-Turbine during Start-up Transient up to Speed No-Load Condition in Generating Mode”, Proceedings of the Institution of Mechanical Engineers, Part A: Journal of Power and Energy, **230**, 6.
- [14] Yang J., Gao L., Wang Z.W., Zhou X.Z., Xu H.X., 2014, “The Flow Field Investigations of No Load Conditions in Axial Flow Fixed-Blade Turbine”, IOP Conference Series: Earth and Environmental Science, **22**, 3, 032028. doi:10.1088/1755-1315/22/3/032028.
- [15] Widmer C., Staubli T., Ledergerber N., 2011, “Unstable Characteristics and Rotating Stall in Turbine Brake Operation of Pump-Turbines”, ASME J. Fluids Eng., **133**, 4.
- [16] Hasmatuchi V., Farhat ., Roth S., Botero F., Avellan F., 2011, “Experimental Evidence of Rotating

- Stall in a Pump-Turbine at off-Design Conditions in Generating Mode”, ASME J. Fluids Eng, **133**, 5.
- [17] Botero, F., V. Hasmatuchi, S. Roth, and M. Farhat., 2014, “Non-Intrusive Detection of Rotating Stall in Pump-Turbines”, Mechanical Systems and Signal Processing, **48**, 162–73.
- [18] Houde S., Fraser R., Ciocan G.D., Deschênes C., 2012, “Experimental study of the pressure fluctuations on propeller turbine runner blades: Part 2, transient conditions”, proc. of 26th IAHR Symposium on Hydraulic Machinery and Systems, Beijing, China.